



Co-existence of LiI and KI in filler-free, quasi-solid-state electrolyte for efficient and stable dye-sensitized solar cell

S. Agarwala^a, L.N.S.A. Thummalakunta^a, C.A. Cook^c, C.K.N. Peh^a, A.S.W. Wong^b, L. Ke^b, G.W. Ho^{a,*}

^a Department of Electrical and Computer Engineering, National University of Singapore, 4 Engineering Drive, Singapore 117576, Singapore

^b Institute of Materials Research and Engineering, A*STAR (Agency for Science Technology and Research), 3 Research Link, Singapore 117602, Singapore

^c Faculty of Applied Science and Engineering, University of Toronto, Toronto, M5S1A4 Canada

ARTICLE INFO

Article history:

Received 25 May 2010

Received in revised form 13 July 2010

Accepted 19 August 2010

Available online 8 September 2010

Keywords:

Quasi-solid-electrolyte

Titanium dioxide

Dye-sensitized solar cell

Light-scattering

Efficiency

ABSTRACT

A quasi-solid-state electrolyte employing a poly (ethylene oxide)/LiI system without a filler is evaluated. The electrolyte is optimized for various potassium iodide (KI) concentrations. The electrolyte containing 14.5 wt.% KI exhibits the highest conductivity ($3.0 \times 10^{-3} \text{ S cm}^{-1}$). An efficiency of 4.5% is achieved using this composition of the electrolyte. It is shown that the introduction of KI in a conventional PEO/LiI electrolyte system prevents the crystallization of the polymer matrix and enhances the ionic conductivity. The energy conversion efficiency of the device is further enhanced to 5.8% by incorporating a light-scattering layer.

© 2010 Elsevier B.V. All rights reserved.

1. Introduction

Dye-sensitized solar cells (DSSCs) are a promising alternatives to silicon solar cells [1–4]. Most DSSC, however, use liquid electrolyte and thus suffer from poor long-term stability caused by evaporation and leakage. Much work has been carried out to prevent or reduce electrolyte leakage, for instance use of composite materials in the electrolyte [5], ionic liquids in place of volatile solvents [6,7], and organic and inorganic hole transport materials [8–11]. Use of solid-state or quasi-solid-state electrolyte is another alternative approach, which is particularly attractive to practical application owing to ease of fabrication, low cost and good stability [12,13].

A typical quasi-solid electrolyte is comprised of a metal salt with low lattice energy dissolved in a polymer matrix. Energy conversion efficiencies of up to 4.2% have been achieved for poly (ethylene oxide) (PEO) based electrolytes [5]. These electrolytes have the inherent limitation of low ionic diffusion, especially in low viscous media, and poor penetration of the electrolyte [14]. In order to enhance the overall conversion efficiency and transport properties of DSSCs, the nature or composition of the electrolytes must be improved. One way is to add organic/inorganic molecules

(plasticizers) to the electrolyte. Inorganic nanoparticles are now commonly used after Croce et al. [15] successfully incorporated titanium dioxide (TiO₂) nanoparticles in the polymer electrolyte. The performance of electrolytes using TiO₂, SiO₂, Al₂O₃ and ZnO has already reached the same level as that of ionic liquid electrolytes [16–20]. Inorganic nanoparticles act as fillers and decrease the degree of crystallization of the polymer matrix. Although, plasticized polymer electrolytes exhibit high efficiencies [21–23], they tend to compromise on the mechanical properties of the electrolyte [24]. Selecting a proper metal salt for the electrolyte is also important. This is because a metal cation of small size easily steers through the dye and tends to intercalate in the pores of the working electrode [25]. Park et al. [26] has shown that a small cation (like Li⁺) leads to a smaller solvated ion cloud, faster diffusion, and higher efficiency. A larger cation (like K⁺) separate causes, better, separation of the polymer chains, thus leading to higher ionic conductivity [27].

The aim of this work is to enhance the ionic conductivity of the polymer electrolyte without compromising the mechanical properties. Thus, a filler-free polymer electrolyte (with metal cations) has been synthesized. Keeping the importance of cation size in mind, both Li⁺ and K⁺ ions are used in the present electrolyte. The intercalation of small Li⁺ ions helps to increase the ionic conductivity since they have a higher dielectric constant. In addition, K⁺ ions assist in separating the polymer chains. An efficient DSSC is made by optimizing the concentration of KI in the electrolyte. Efficiency is further enhanced through the addition of a scattering layer.

* Corresponding author at: Engineering Science, EA 07-37, Blk E3A #04-17, National University of Singapore, Singapore 117574, Singapore.
Tel.: +65 6516 8121; fax: +65 6516779.

E-mail address: elehw@nus.edu.sg (G.W. Ho).

2. Experimental procedures

2.1. Electrolyte preparation

The polymer electrolyte was prepared by adding 0.264 g of PEO ($M_w \sim 200,000$) to 50 ml of acetonitrile. 0.1 g of lithium iodide (LiI) and 0.019 g of iodine were then added to the mixture under continuous stirring. Finally, potassium iodide (KI) was added. A total of six electrolyte solutions were made, with the KI content varying from 10.5 to 20.5 wt.%. The electrolytes were stirred continuously overnight. All the electrolytes were heated ($\sim 70^\circ\text{C}$) to evaporate the solvent, up to the point that the final product had a gel-like character.

2.2. TiO_2 nanoparticle synthesis ($\text{TiO}_2\text{-NP}$)

Grätzel's method [1] was used for the preparation of TiO_2 nanoparticles. 1 ml of 0.1 M nitric acid was added to 40 ml of titanium (IV) isopropoxide under constant stirring and the resulting solution was heated to 90°C for 8 h. The mixture was cooled down to room temperature and filtered. The filtrate was heated in an autoclave at 240°C for 12 h. The solution was then dried and converted into powder.

2.3. Synthesis of TiO_2 scattering particles ($\text{TiO}_2\text{-SP}$)

For synthesis of the scattering layer of TiO_2 , 0.5 ml tetrabutoxytitanium (TBT) was added to 10 ml of ethylene glycol under nitrogen purging. The solution was magnetically stirred overnight at room temperature, and the poured into an acetone bath (~ 120 ml) containing 0.3 ml of de-ionized (DI) water, under vigorous stirring. The white precipitate was separated using centrifugation, followed by repeated washing with DI water and ethanol. This step was necessary to ensure removal of ethylene glycol from the surfaces of the titanium dioxide glycolate particles. The particles were converted to pure anatase TiO_2 by annealing in air at 450°C for 30 min.

2.4. Solar cell assembly

$\text{TiO}_2\text{-NP}$ was converted into a fine paste using DI water without any binder, and then spread on fluorine doped tin oxide (FTO) glass (resistivity 15 cm^{-2}) by the 'Doctor Blade' technique (cell area 0.25 cm^2). Only one layer of scotch tape ($\sim 40\ \mu\text{m}$ thickness) was used for all the electrodes. The film was allowed to dry in ambient conditions before heating at 450°C for 30 min in air. To make the DSSCs the films were immersed in an ethanolic solution containing 0.3 mM Ru-dye, *cis*-dithiocyanate-*N,N'*-bis(4-carboxylate-4-tetrabutylammoniumcarboxylate-2,2'-bipyridine) ruthenium (II) (known as N719, Solaronix), for 24 h at room temperature. Subsequently, the films were rinsed with ethanol. The electrolyte was injected through a hole in the platinum-coated counter electrode, and the hole was then sealed with hot-melt surlyn (Solaronix) film. Two different types of device were prepared for testing. The first device (D1) had a working electrode of only $\text{TiO}_2\text{-NP}$, while the second device (D2) had an additional top layer of $\text{TiO}_2\text{-SP}$, which was spin coated at 3000 rpm. The aim was to have an outer layer with strong light-scattering ability.

2.5. Analysis techniques

The morphology of synthesized TiO_2 films was examined with a JEOL-2100 high-resolution transmission electron microscope (HRTEM) with an accelerating voltage of 200 kV and with a JEOL FEG JSM 6700 F field-emission scanning electron microscope (FESEM) operating at 10 kV. Film thickness was determined with a Ambios Technology XP 200 profilometer. Structural characterization of the

synthesized films was obtained by means of X-ray diffraction (XRD) on Philips X-ray diffractometer with $\text{Cu K}\alpha$ radiation ($\lambda = 1.541\ \text{\AA}$). Brunauer–Emmett–Teller (BET) measurements were conducted using a Quantachrome Nova 1200 limit with N_2 as the adsorbate at liquid nitrogen temperature. The photocurrent–voltage of the samples was measured with a solar simulator (Newport 91160A) equipped with an Author to define AM filter and a 150 W Xe lamp as the light source. The solar cells were tested at 25°C with a source meter (Keithley 2420) using Newport IV test station software. The light intensity corresponding to AM 1.5 (100 mW cm^{-2}) was calibrated using a standard silicon solar cell (Oriel, SRC-1000-TC). Incident photon-to-collected-electron conversion efficiency (IPCE) spectra were measured with a spectral resolution of 5 nm using a 300 W Xenon lamp and a grating monochromator equipped with order sorting filters (Newport/Oriel). The incident photon flux was determined using a calibrated silicon photodiode (Newport/Oriel). Control of the monochromator and recording of photocurrent spectra were performed using TRACQ Basic software (Newport). Electrochemical impedance spectroscopy (EIS) was recorded with a potentiostat PGSTAT 302N (Autolab, Eco Chemie, The Netherlands) under an illumination of 100 mW cm^{-2} . The frequency range was varied from 0.05 Hz to 100 KHz and magnitude of the alternating signal was 10 mV. The conductivity of the PEO/LiI/KI system was derived from the complex impedance measurements. The conductivity (σ) of the polymer complex films was calculated using the following equation

$$\sigma = \frac{L}{AR_b} \quad (1)$$

where R_b is the bulk resistance determined from the intersection of the high-frequency semicircle with the real axis in complex impedance plots; L is the thickness of the film; A is the area of the sample.

3. Results and discussion

3.1. Characterization of $\text{TiO}_2\text{-NP}$ and $\text{TiO}_2\text{-SP}$ films

The SEM images of $\text{TiO}_2\text{-SP}$ prepared from four different concentrations of TBT in acetone are shown in Fig. 1 a. The diameter and density of the nanoparticles can be easily tuned by changing the concentration of TBT. When 0.05, 0.1 and 0.5 ml TBT is used, well-dispersed uniform and spherical nanoparticles are obtained. This uniformity can be attributed to ethylene glycol which reduces the hydrolysis rate of TBT. As observed, the diameter of these particles increases with the amount of TBT (from 50 to 130 nm). This is due to an increased number of nuclei present to form titanium glycolate. With further increase in TBT, the particles tend to fuse together and form larger agglomerates. The TBT concentration of 0.5 ml in 120 ml acetone gives poly-dispersed particles with the largest diameter in the range of 90–130 nm. Hence, this concentration of TBT is used to prepare the light-scattering layer for the DSSC. The spherical nature of the $\text{TiO}_2\text{-SP}$ is also confirmed by TEM. The TEM image of the particles after annealing at 450°C for 30 min is shown in Fig. 1b. The image clearly shows that the spherical morphology of the particles is essentially preserved during the annealing process. An SEM of the $\text{TiO}_2\text{-NP}$ film after sintering at 450°C for 30 min is displayed in Fig. 1c. The film is composed of aggregates of smaller particles in the size range of 15–20 nm. Small grains with dense structures are observed in the micrographs. These particles are mostly square in shape (Fig. 1d). BET analysis shows the total surface area of the $\text{TiO}_2\text{-NP}$ and $\text{TiO}_2\text{-SP}$ 105.0 and $39.4\text{ m}^2\text{ g}^{-1}$, respectively.

The XRD pattern of $\text{TiO}_2\text{-NP}$ and $\text{TiO}_2\text{-SP}$ films after annealing at 450°C for 30 min are depicted in Fig. 2. For $\text{TiO}_2\text{-SP}$, the sample containing 0.5 ml TBT was chosen. Both the patterns display well-resolved and sharp peaks. It is clear that both particles

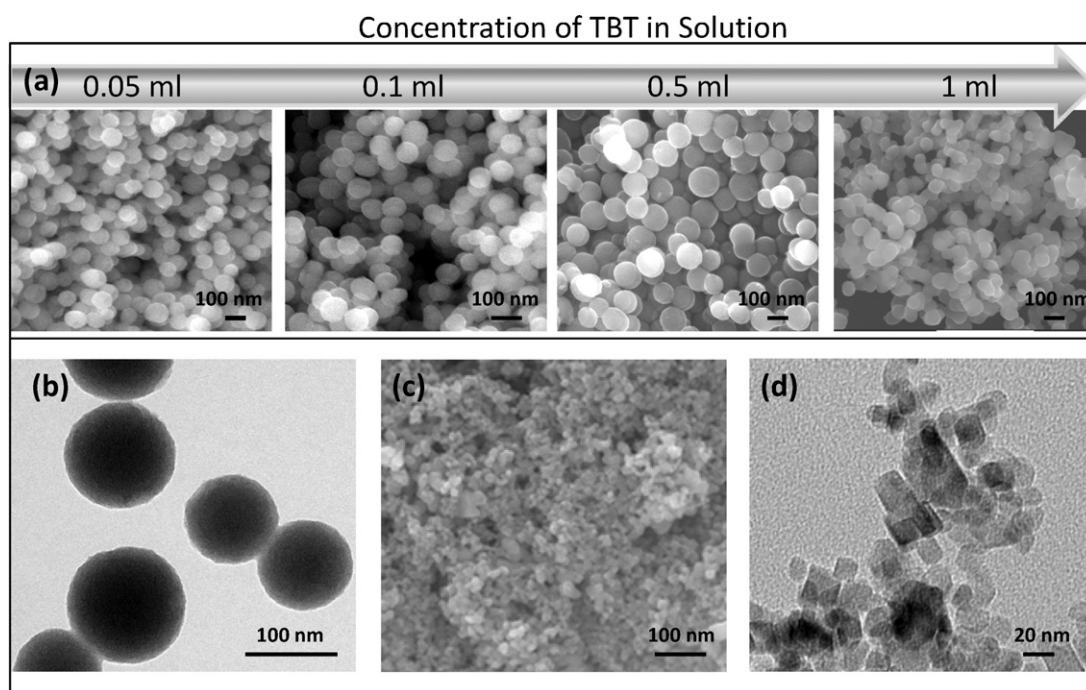


Fig. 1. (a) SEM images at different TBT concentrations and (b) TEM images of $\text{TiO}_2\text{-SP}$. (c) SEM and (d) TEM of $\text{TiO}_2\text{-NP}$ film.

are polycrystalline in nature and have anatase as the predominant phase. The peaks are indexed corresponding to the (101), (004), (200) and (105) anatase phase of TiO_2 (JCPDS file no. 21-1272). A small amount of (110) rutile phase was also present in $\text{TiO}_2\text{-SP}$ (JCPDS file no. 21-1276).

3.2. Electrolyte characterization

It is well known that the conductivity of PEO-blended electrolytes containing metal salts increases with the size of the cation [28]. The ionic conductivity of the electrolyte, however, also depends on many other factors. The total conductivity of an electrolyte can be expressed by the following equation:

$$\sigma = n \cdot q \cdot \mu \quad (2)$$

where n is the density of charge carriers; q is the number of electron charges per one carrier; μ is the mobility of the carriers. Dissociated carriers (n) are in turn related to the dissociation energy (U) and

dielectric constant (ϵ) as follows [29]:

$$n = n_0 \exp \left[\frac{-U}{2s k_B T} \right] \quad (3)$$

where k_B is the Boltzmann constant and T is the absolute temperature. Hence, ionic conductivity can be enhanced by incorporating metal salts that have larger ionic radii, higher mobilities, higher dielectric constants and lower dissociation energies. The ionic radius of the K^+ ions (1.38 Å) is larger than that of Li^+ ions (0.76 Å) [30]. Hence, it is expected that K^+ ions would have higher ionic conductivity. K^+ ions have lower ϵ (596.34) than Li^+ ions (722.95) which will tend to lower the ionic conductivity. Hence, it was decided to incorporate both the metal ions in the polymer chain to balance out the negative effects of both. The cations of Li^+ become adsorbed on the TiO_2 layer [20] and help increase the ionic conductivity through a higher dielectric constant value. The K^+ ions are attracted to the ether oxygen [21] and help to make the polymer more amorphous. Adding larger K^+ ions to the electrolyte helps to decrease the crystallization of the PEO polymer, thus acting as filler.

The photocurrent density–voltage characteristics of the cells made with different KI concentrations in the electrolyte under simulated irradiation (global AM 1.5) are displayed in Fig. 3. It is found that the short-circuit current density (J_{sc}) increases with the KI weight percentage. For the PEO-based electrolytes, the ionic conductivity is governed by the transport of I^- ions [31]. The increased J_{sc} is attributed to decreased crystallinity in the polymer chain that leads to enhanced charge transfer. The highest J_{sc} (9.10 mA cm^{-2}) is reported for 14.5 wt.% KI. The inset of Fig. 3 shows the trend of conversion efficiency with different KI concentrations. The J_{sc} decrease when the KI concentration is increased beyond 14.5 wt.%. This may be due to formation of ion pairs and cross-linking sites that hinder the motion of the ions in the polymer chain and reduce the ionic mobility [32]. Table 1 summarizes the solar cell performance parameters obtained for different KI concentrations.

The XRD pattern of the quasi-solid-state electrolyte with varying amount of KI is shown in Fig. 4. The electrolyte without KI has sharp and well-defined peaks at 26.8, 34.0, 38.2, 51.9, 60.9 and

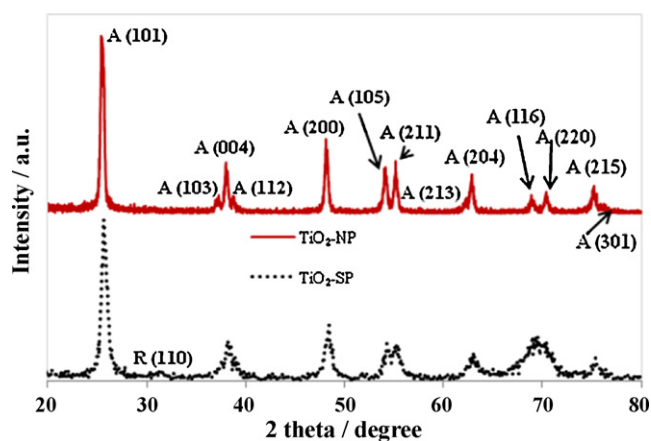


Fig. 2. XRD spectra of $\text{TiO}_2\text{-NP}$ and $\text{TiO}_2\text{-SP}$ films. 'A' represents anatase and 'R' rutile phase of TiO_2 .

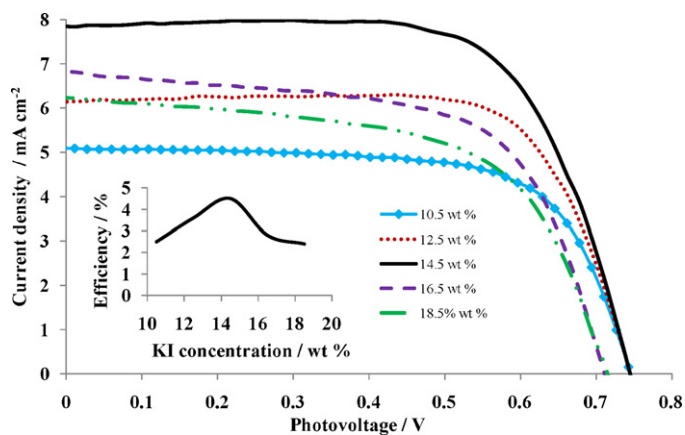


Fig. 3. I - V curves for DSSC using quasi-solid electrolyte at various KI loading. Inset shows calculated cell efficiencies at different wt.% KI.

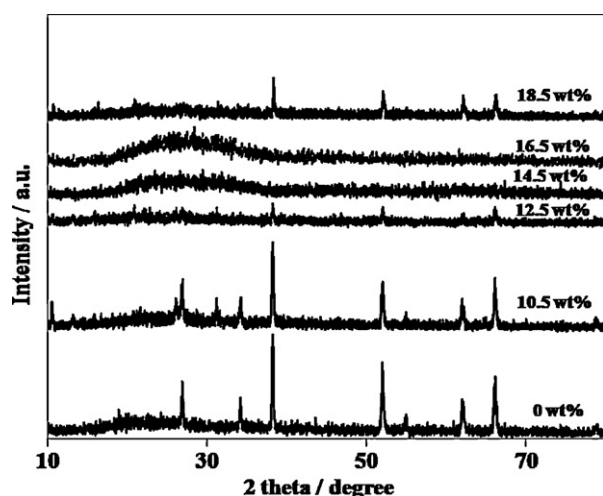


Fig. 4. XRD spectra of PEO/LiI based electrolyte with various KI loading.

62.1°, which indicate a semi-crystalline nature. The crystalline peak intensities are progressively decreased with increase in the KI concentration, and nearly vanish at 14.5 wt.%. This suggests that KI does prevent PEO from crystallizing. The reduced crystallinity of PEO is due to interaction of KI with the ether oxygen of the polymer chain. The increased amorphous phase of PEO with 14.5 wt.% KI will favour inter- and intra-chain ion movements and improve the electrical conduction. Further addition of KI causes agglomeration and phase separation, thus increasing the crystallinity and the I^-/I_3^- diffusion resistance of the electrolyte.

The room temperature ionic conductivity (σ) of the PEO/ I_2 /LiI/KI (14.5 wt.% KI) system is compared with pure polymer PEO/ I_2 /LiI, PEO/ I_2 /KI and PEO/ I_2 /LiI/ TiO_2 systems. All the electrolytes (film thickness $\sim 100 \mu\text{m}$) are deposited on Pt-coated FTO glasses, using a spacer ($\sim 0.05 \text{ mm}$). The values of the ionic conductivities are listed in Table 2. The ionic conductivities of the pure polymer and plasticized electrolyte systems are close to those reported in literature

Table 1
DSSC performance at various KI loadings in quasi-solid electrolyte.

KI concentration (wt.%)	V_{oc} (V)	J_{sc} (mA cm^{-2})	FF (%)	Efficiency (%)	R at V_{oc} (Ω)
10.5	0.6	5.5	67.5	2.5	67.0
12.5	0.7	6.7	73.0	3.6	65.8
14.5	0.7	9.1	66.2	4.5	59.7
16.5	0.6	6.8	62.3	2.8	63.7
18.5	0.6	6.2	59.4	2.4	73.0

Table 2
Computed ionic conductivity values for various electrolyte systems.

Electrolyte	σ (S cm^{-1})
PEO/ I_2 /LiI	1.9×10^{-5}
PEO/ I_2 /KI	5.6×10^{-5}
PEO/ I_2 /LiI/ TiO_2	2.0×10^{-3}
PEO/ I_2 /LiI/KI	3.0×10^{-3}

Table 3
Photovoltaic characteristics for cells made from 14.5 wt.% KI electrolyte measured under illumination with AM 1.5 simulated sunlight.

DSSC	V_{oc} (V)	J_{sc} (mA cm^{-2})	FF (%)	Efficiency (%)
D1	0.7	9.1	66.2	4.5
D2	0.6	12.6	71.0	5.8

[27,33,34]. The optimized electrolyte with 14.5% KI in the PEO/ I_2 /LiI matrix gives a conductivity value of $3.0 \times 10^{-3} \text{ S cm}^{-1}$, which is much higher than polymer and metal salt matrix electrolytes. The ionic conductivity of 14.5 wt.% KI is almost comparable with that achieved by adding TiO_2 filler. Hence, this study demonstrates an enhancement in the ionic conductivity of the polymer electrolyte without incorporating any inorganic fillers. It is already well-established that fillers tend to decrease the mechanical strength of the polymer electrolytes. The enhancement in ionic conductivity for a PEO/ I_2 /LiI/KI electrolyte comes from K^+ ions acting as fillers to reduce the crystallization of the PEO polymer chains. Hence, K^+ ions act as supplement for the inorganic fillers. The low dielectric constant of Li^+ ions promotes the ionic conductivity of the electrolyte. On the other hand, the K^+ ions (whose size is larger than Li^+ ions) become attracted to the ether oxygen [35] and render the polymer more amorphous. The K^+ ions interact with the ethylene oxide repeating units of the PEO polymer through Lewis type acid-base interactions.

3.3. DSSC Performance with TiO_2 -SP and quasi-solid electrolyte

To enhance the conversion efficiency of DSSC, a 300 nm thick scattering layer (TiO_2 -SP) is coated on TiO_2 -NP electrode. The photovoltaic performances of the device D1 (without scattering layer) and D2 (with scattering layer) are shown in Fig. 5a. An increase of 29% is recorded in the conversion efficiency with D2 compared with D1. For the same quasi-solid electrolyte, the energy conversion efficiency is increased to 5.8% for D2. The improved photovoltaic performance is mainly due to increased J_{sc} and fill factor. An enhanced J_{sc} is attributed to better dye loading and increased light harvesting capability of the film. TiO_2 -SP particles ($\sim 100 \text{ nm}$) also promote better penetration of the dye, which reduces the series resistance of device. The enhanced fill factor is linked to the rapid diffusion of the polymer electrolyte in the TiO_2 film. The photovoltage decreases due to poor connectivity between the FTO and the electrolyte. A summary of the various solar cell parameters is given in Table 3. The inset of Fig. 5a shows the incident photo-current conversion efficiency (IPCE) obtained for D1 and D2. It is well-known that light of a shorter wavelength is relatively more scattered on a rough surface than that of longer wavelength. This is because the scattering efficiency of light is proportional to

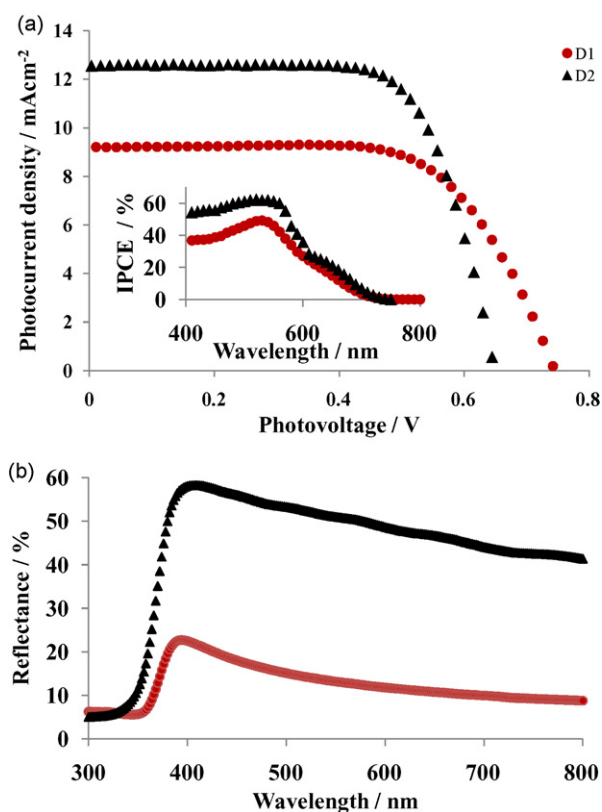


Fig. 5. (a) I - V characteristics and (b) reflectance spectra of DSSC with and without TiO_2 -SP layer. Inset shows IPCE of DSSC.

λ^{-4} , where λ is the wavelength of incident light. The IPCE spectra indicate that the improvement of quantum efficiency for D2 is relatively higher in the shorter wavelength region (400–600 nm) than at longer wavelengths.

The light-scattering properties of the synthesized TiO_2 films are investigated with diffuse reflectance spectra, as shown in Fig. 5b. A considerable increase in the reflectance can be observed after the addition of 100 nm TiO_2 -SP particles in the D2 electrode. TiO_2 -SP exhibits high reflectance in the whole visible region (400–800 nm). The reflection for D1 and D2 reduces dramatically under 400 nm because of the light absorption caused by the band transition of TiO_2 (band gap 3.0 eV).

3.4. Reproducibility and stability of DSSC

In order to determine the factors that influence the stability of the quasi-solid-state electrolyte DSSC, EIS spectra were measured. The Nyquist plots for the fresh and days aged sample (5 days) are shown in Fig. 6a. As expected, the aged device shows higher diffuse-related resistance and electron transport resistance compared with the fresh device. Also, in the kinetic region, the fresh device shows a blue shift in the peak related to the electrolyte diffusion, and thereby suggests more rapid charge transfer than for the aged device. With time, the solvent tends to evaporate and hence the polymer chains start to crystallize and lead to poor ionic conductivity in the device. The inset of Fig. 6a shows the equivalent circuit

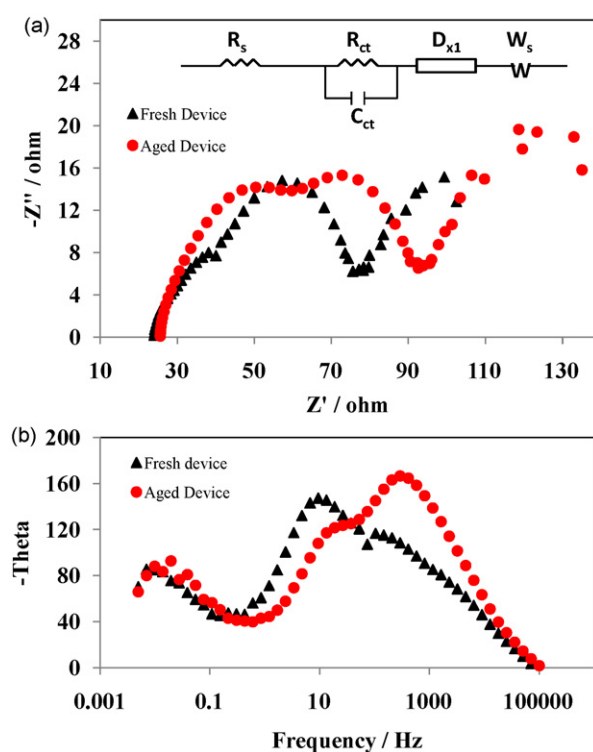


Fig. 6. (a) Nyquist plots and (b) Bode plots of fresh and aged quasi-solid-state DSSC. Inset shows equivalent circuit model of DSSC.

model of the impedance of the quasi-solid-electrolyte DSSC. The transmission line model is used where R_s describes the resistance of the quasi-solid electrolyte, R_{ct} and C_{ct} describe the recombination resistance and the chemical capacitance of the DSSC respectively, D_{x1} relates to the interface of the photoelectrode and the electrolyte, W_s encompasses the finite Warburg impedance elements associated with the diffusion of tri-iodide in the electrolyte, and R_{diff} is the diffusion resistance of the I^-/I_3^- in the quasi-solid electrolyte. Ageing of the DSSC mainly affects R_{ct} and R_{diff} , whose values change by twice the initial value. Hence, the loss in DSSC efficiency can be attributed to degradation of the electrolyte over time, which tends to increase the recombination in the device. The Bode phase plots of the EIS spectra (Fig. 6b) display the frequency peaks of the charge-transfer process at different interfaces for the two devices. The electron lifetime for the recombination (τ_e) in the devices is determined by the equation, $\tau_e = 1/\omega_{\min} = 1/2\pi f_{\max}$. Table 4 summarizes the quantitatively fitted results using the equivalent circuit model. It is observed that the fresh device exhibits lower values for R_s and R_{diff} , implying a more efficient charge-transfer process at the TiO_2 /electrolyte interface and the Pt counter electrode/redox electrolyte interface. The circuit model uses constant-phase elements of the capacitance (CPE). This comes from the non-ideal frequency-dependent capacitance arising from the non-uniform distribution of the current by the material heterogeneity [36]. The CPE is defined by two values, CPE-T and CPE-P, the latter is a constant that ranges from 0 to 1. The results show a CPE-P value of 1 which is caused by the appearance of a double-layer capacitance due to the rough and porous surface of the photoelectrode [36]. From the above dis-

Table 4
Fitted impedance parameters for the fresh and aged DSSC with 14.5 wt.% KI in the electrolyte.

D2	Film thickness (μm)	R_s (Ω)	R_{ct} (Ω)	R_{diff} (Ω)	C_{ct} (μF)	τ_e (ms)	D ($\text{cm}^2 \text{s}^{-1}$)
Fresh device	9.0	23.7	16.7	23.8	21.0	23.0	3.2×10^{-5}
Aged device	9.0	24.5	6.3	42.5	24.4	11.0	1.8×10^{-5}

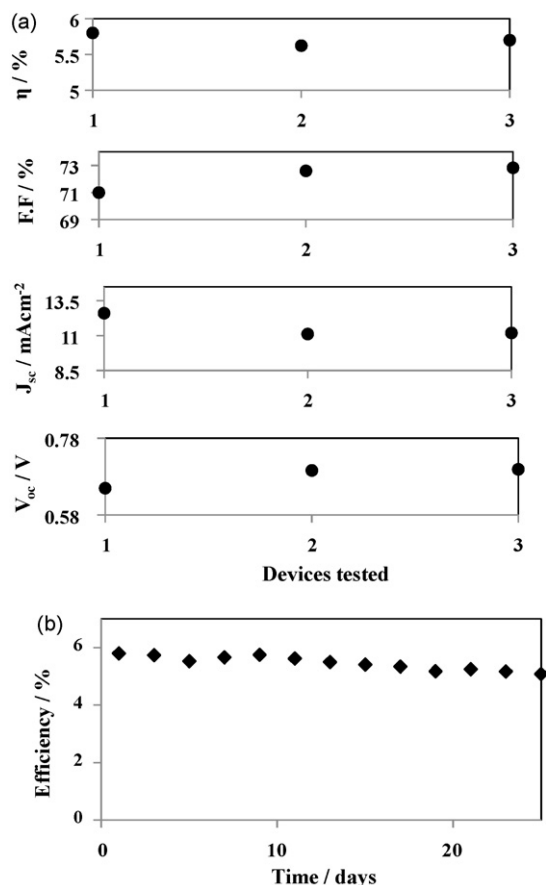


Fig. 7. (a) DSSC performance of three devices which were tested for reproducibility. (b) Stability for quasi-solid-state DSSC containing KI in electrolyte and TiO₂-SP layer in photoelectrode.

discussion, it is concluded that with ageing the overall resistance of the device increases (due to crystallization of the polymer matrix), which leads to shorter electron lifetime and higher electron recombination in the device. In summary, the stability of the device with quasi-solid electrolyte is much better than that observed with liquid electrolytes.

In order to ascertain the reproducibility, three different devices from different batches of materials were made and tested. The trend of the various DSSC parameters obtained for the tested devices is shown in Fig. 7a. Device D2 incorporating TiO₂-SP with a quasi-solid-state electrolyte is also tested for stability. An evaluation of the efficiency during the ageing period for D2 is given in Fig. 7b. The cell performance is evaluated at specific intervals and after the evaluation the cell is stored in the desiccator cabinet at room temperature. The cell efficiency starts to decrease initially. This may be due to evaporation of solvent in the electrolyte. After 9 days, the cell's efficiency increases slightly as the polymer electrolyte penetrates deeper into the porous TiO₂ electrode. D2 loses 12.2% of its initial efficiency after a period of 25 days.

4. Conclusions

The addition of KI to a PEO/LiI polymer electrolyte to increase the ionic conductivity is demonstrated. The concentration of KI is optimized to obtain a high-efficiency DSSC. 14.5 wt.% KI yields a homogeneous polymer electrolyte with the conductivity of the

order $3 \times 10^{-3} \text{ S cm}^{-1}$ and energy conversion efficiency of 4.5%. Further increase in the KI concentration causes a drop in the DSSC efficiency due to the formation of cross-linking networks in the electrolyte, as confirmed by XRD. To enhance further the DSSC performance, an additional light-scattering layer of $\sim 100 \text{ nm}$ particles of anatase TiO₂ is introduced. The short-circuit current density of the DSSC thus increases to 12.6 mA cm^{-2} . This can be attributed to the light-scattering effect of the TiO₂ electrode film. An energy conversion efficiency of 5.8% is obtained by employing a light-scattering layer with the KI incorporated polymer electrolyte.

Acknowledgment

This work was supported by Applied Materials.

References

- [1] B. O'Regan, M. Grätzel, *Nature* 353 (1991) 737–740.
- [2] M.K. Nazeeruddin, A. Kay, I. Rodicio, R. Humphrybaker, E. Muller, P. Liska, N. Vlachopoulos, M. Grätzel, *J. Am. Chem. Soc.* 115 (1993) 6382–6390.
- [3] F.C. Krebs, M. Biancardo, *Solar Energy Mater. Solar Cells* 90 (2006) 142–165.
- [4] P. Wang, S.M. Zakeeruddin, J.E. Moser, R. Humphry-Baker, P. Comte, V. Aranyos, A. Hagfeldt, M.K. Nazeeruddin, M. Grätzel, *Adv. Mater.* 16 (2004) 1806–1811.
- [5] T. Stergiopoulos, I.M. Arabatzis, G. Katsaros, P. Falaras, *Nano Lett.* 2 (2002) 1259–1261.
- [6] P. Wang, S.M. Zakeeruddin, J.-E. Moser, M. Grätzel, *J. Phys. Chem. B* 107 (2003) 13280–13285.
- [7] R. Kawano, H. Matsui, C. Matsuyama, A. Sato, Md.A.B.H. Susan, N. Tanabe, M. Watanabe, *J. Photochem. Photobiol. A: Chem.* 164 (2004) 87–92.
- [8] N. Ikeda, K. Teshima, T. Miyasaka, *Chem. Commun.* 16 (2006) 1733–1735.
- [9] B. O'Regan, F. Lenzmann, R. Muis, J. Wienke, *Chem. Mater.* 14 (2002) 5023–5029.
- [10] S. Murai, S. Mikoshiba, H. Sumino, T. Kato, S. Hayase, *Chem. Commun.* 13 (2003) 1534–1535.
- [11] B. O'Regan, D.T. Schwartz, *Chem. Mater.* 10 (1998) 1501–1509.
- [12] J. Krüger, R. Plass, L. Cevey, M. Picirelli, M. Grätzel, U. Bach, *Appl. Phys. Lett.* 79 (2001) 2085–2087.
- [13] E. Stathatos, P. Lianos, S.M. Zakeeruddin, P. Liska, M. Grätzel, *Chem. Mater.* 15 (2003) 1825–1829.
- [14] T. Kato, A. Okazaki, S. Hayase, *Chem. Commun.* 3 (2002) 363–365.
- [15] F. Croce, G.B. Appetecchi, L. Persi, B. Scrosati, *Nature* 394 (1998) 456–458.
- [16] P. Wang, S.M. Zakeeruddin, P. Comte, I. Exnar, M. Grätzel, *J. Am. Chem. Soc.* 125 (2003) 1166–1167.
- [17] H. Han, U. Bach, Y.-B. Cheng, R.A. Caruso, *Appl. Phys. Lett.* 90 (2007) 213510.
- [18] J. Zhang, H. Han, S. Wu, S. Xu, Y. Yang, C. Zhou, X. Zhao, *Solid State Ionics* 178 (2007) 1595–1601.
- [19] X. Zhang, H. Yang, H.M. Xiong, F.Y. Li, Y.Y. Xia, *J. Power Sources* 160 (2006) 1451–1455.
- [20] G. Nazmutdinova, S. Sensfuss, M. Schrödner, A. Hinsch, R. Sastrawan, D. Gerhard, S. Himmeler, P. Wasserscheid, *Solid State Ionics* 177 (2006) 3141–3146.
- [21] J.N. De Freitas, V.C. Nogueira, B.I. Ito, M.A. Soto-Oviedo, C. Longo, M.-A. De Paoli, A.F. Nogueira, *Int. J. Photoenergy* 75483 (2006) 1–6.
- [22] M.S. Kang, K.S. Ahn, J.W. Lee, *J. Power Sources* 180 (2008) 896–901.
- [23] C.W. Tu, K.Y. Liu, A.T. Chien, M.H. Yen, T.H. Weng, K.C. Ho, K.F. Lin, *J. Polym. Sci. A: Polym. Chem.* 46 (2008) 47–53.
- [24] J.N. De Freitas, A.F. Nogueira, M.-A. De Paoli, *J. Mater. Chem.* 19 (2009) 5279–5294.
- [25] H. Wang, J. Bell, J. Desilvestro, M. Bertoz, G. Evans, *J. Phys. Chem. C* 111 (2007) 15125–15131.
- [26] N.G. Park, S.H. Chang, J. van de Lagemaat, K.J. Kim, A.J. Frank, *Bull. Korean Chem. Soc.* 21 (2000) 985–988.
- [27] G.P. Kalaignan, M.S. Kang, Y.S. Kang, *Solid State Ionics* 177 (2006) 1091–1097.
- [28] B. Bhattacharya, J.Y. Lee, J. Geng, H.-T. Jung, J.-K. Park, *Langmuir* 25 (2009) 3276–3281.
- [29] R.E. Barker, C.R. Thomas, *J. Appl. Phys.* 35 (1964) 3203–3215.
- [30] J.A. Dean, *Lange's Handbook of Chemistry*, 14th ed., Mc Graw-Hill, New York, 1992.
- [31] Y. Yang, J. Zhang, C.H. Zhou, S.J. Wu, S. Xu, W. Liu, H.W. Han, B.L. Chen, X.-Z. Zhao, *J. Phys. Chem. B* 112 (2008) 6594–6602.
- [32] G.G. Silva, N.H.T. Lemes, C.N. Polo Da Fonseca, M.-A. De Paoli, *Solid State Ionics* 93 (1996) 105–116.
- [33] C.A. Vincent, *Prog. Solid State Chem.* 17 (1987) 145–261.
- [34] A.G. Kontos, M. Fardis, M.I. Prodromidis, T. Stergiopoulos, E. Chatzivasiloglou, G. Papavassiliou, P. Falaras, *Phys. Chem. Chem. Phys.* 8 (2006) 767–776.
- [35] X. Shen, W. Xu, J. Xu, G. Liang, H. Yang, M. Yao, *Solid State Ionics* 179 (2008) 2027–2030.
- [36] Q. Wang, J.-E. Moser, M. Grätzel, *J. Phys. Chem. B* 109 (2005) 14945–14953.